analytical chemistry

pubs.acs.org/ac

Article

Molecular Characterization of Organophosphorus Compounds in Wildfire Smoke Using 21-T Fourier Transform-Ion Cyclotron Resonance Mass Spectrometry

Amna Ijaz,* William Kew, Swarup China, Simeon K. Schum, and Lynn R. Mazzoleni*

Cite This: *Anal. Chem.* 2022, 94, 14537−14545

Read Online

ACCESS | Metrics & More | Article Recommendations | Supporting Information

ABSTRACT: We present a detailed molecular characterization of organophosphorus compounds in ambient organic aerosol influenced by wildfire smoke. Biomass burning organic aerosol (BBOA) is an important source of phosphorus (P) to surface waters, where even a small imbalance in the P flux can lead to substantial effects on water quality, such as eutrophication, algal blooms, and oxygen depletion. We aimed to exploit the ultrahigh resolving power, mass accuracy, and sensitivity of Fourier transform-ion cyclotron resonance mass spectrometry (FT-ICR MS) to explore the molecular composition of an ambient BBOA sample collected downwind of Pacific Northwest wildfires. The 21-T FT-ICR MS yielded 10 533 distinct formulae, which included molecular species comprising C, H, O, and P with or without N, i.e., organophosphorus compounds that have long been quantified in wildfire smoke but have not yet been characterized at the molecular level. The lack of detailed molecular characterization of organophosphorus compounds in BBOA is primarily due to their inherently low concentrations in aerosols and poor ionization efficiency in complex mixtures. We demonstrate that the exceptional sensitivity of the 21-T FT-ICR MS allows qualitative analysis of a previously uncharacterized fraction of BBOA without its selective concentration from the organic matrix, exemplifying the need for ultrahigh-resolution tools for a more detailed and accurate molecular depiction of such complex mixtures.

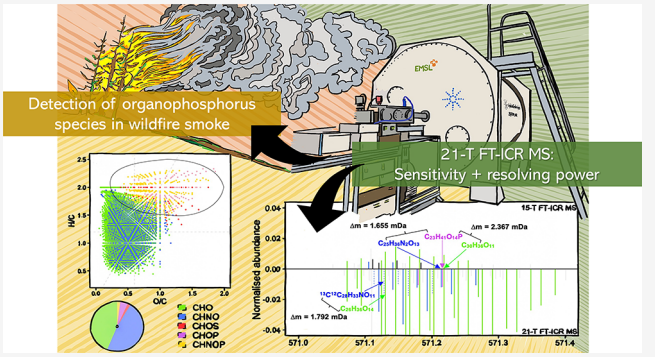

Atmospheric aerosols play a central role in controlling our planet's radiative balance, biogeochemical cycling, air quality, and human health, due to which they constitute one of the nine planetary variables[1] that must be regulated globally to limit human impact on the climate and environment. Large-scale biomass burning events, such as wildfires, contribute substantially to total organic mass loading in the atmosphere.[2−5] The chemical nature of biomass burning organic aerosol (BBOA) is one of the determinative factors behind its influence on climate and the biotic/abiotic entities that it interacts with. Phosphorus (P)-containing atmospheric aerosols are an important source of P to surface waters via wet and dry atmospheric deposition.[6,7] Phosphorus is an essential nutrient that can limit primary production and nitrogen (N) fixation despite its diffused and minor influx into surface water via aerosols; it can alter the biogeochemical balance of aquatic ecosystems leading to eutrophication, algal blooms, and/or oxygen (O) depletion.[6,8,9] A total of 3.7 Tg P/year is estimated to be emitted globally by a variety of sources,[10] including soil and desert dust, primary biological and marine aerosols, coal combustion, biomass burning, and agricultural fertilizers;[11−13] 20% (0.7−0.8 Tg P/year) of this P is projected to originate from natural fires.[10] Only a small fraction of P (9 Gg/year) directly emitted from large-scale biomass burning events is soluble in water. However, atmospheric aging by the uptake of oxidants during long-range transport converts insoluble organic phosphorus to soluble forms, making it a non-negligible source of bioavailable P to surface waters.[14] Based on simulation studies, Myriokefalitakis et al.[14] estimated bioavailable atmospheric P from biomass burning to have increased by 28% since 1850, with a further 22% increase expected by the year 2100. These predictions are not unprecedented, considering that an increased occurrence of wildfires globally is expected in the future, owing to a warmer, drier climate and changes in fuel availability.[15]

It is well established that P is emitted in substantial quantities from biomass burning and can exert a profound influence on aquatic ecosystems; however, its molecular composition is unknown because only a few studies have

Received: February 25, 2022
Accepted: September 16, 2022
Published: October 10, 2022

included P along with C, H, O, N, and S in ultrahigh-resolution mass spectrometry (ultra-HRMS) analyses of organic aerosols.[16,17] Even in such studies, P-containing formulae were removed from analyses due to their quantitative insignificance among other molecular groups (CHO, CHNO, CHOS, CHNOS, etc.). Given that molecular-level characterization of organophosphorus compounds can provide insight into their aromaticity,[18,19] molecular weight, and elemental ratios, their better representation in HRMS studies on BBOA is warranted. However, a major limitation to mass spectrometric analyses of organophosphorus compounds in complex mixtures is the inefficient ionization of phosphate functional group (PO_4^{3-}) by electrospray ionization (ESI), especially when organophosphates are present in relatively minute quantities among an overwhelming background of non-P organic matter containing competing functional groups, such as carboxylic, carbonyl, and phenolic members.[20] Studies targeting dissolved organic phosphorus (DOP) in natural aquatic organic matter have suggested selective isolation and concentration of DOP prior to ESI and HRMS analysis,[20−22] which is typically not a feasible option for atmospheric aerosol due to limited amounts of sample. Highly oxygenated P-containing species were recently observed in solid-phase extracted dew water using (−)ESI and 12-T Fourier transform-ion cyclotron resonance mass spectrometry (FT-ICR MS), where they were speculated to originate from DNA, phospholipids, and reactions of P-metabolites exuded on the surface of leaves.[23] However, such inclusion of organophosphorus compounds in the molecular characterization of BBOA is yet to be performed.

We present the molecular-level composition of a wildfire-influenced BBOA sample with (−)ESI coupled with a 21-T FT-ICR MS. This mass spectrometer has the greatest magnetic field strength reported to date,[24,25] which affords it a unique blend of high resolving power (RP), sensitivity, acquisition speed, mass accuracy, and dynamic range. The 21-T FT-ICR MS employed here was custom-built at the Pacific Northwest National Laboratory (PNNL), Richland, WA; its detailed design and initial performance have been reported elsewhere.[25] The RP and rate of spectral acquisition of FT-ICR instruments are linearly proportional to their magnetic field strength, while mass accuracy and dynamic range are quadratically related to it.[26] Furthermore, a stronger magnetic field allows large populations of ions to be trapped in the ICR cell before coalescing.[27] Altogether, these properties extend the analytical capabilities of high-field FT-ICR instruments to extract more information from complex mixtures. Here, molecular characterization of the BBOA sample using the 21-T FT-ICR MS led to the detection of P-containing species despite no prior selective concentration of organophosphorus compounds. These constituents were not observed in a parallel characterization performed with another state-of-the-art instrument: 15-T FT-ICR MS. Organophosphorus compounds have long been quantitively reported in wildfire smoke but have never been molecularly characterized with confidence,[16,17] and thus, are the focus of this report to exemplify the importance of subjecting atmospheric BBOA to ultra-HRMS to advance the knowledge on its fine-scale nature and minor constituents.

EXPERIMENTAL SECTION

Sample Collection and Preparation. Aerosol samples were collected on 0.1-μm 90-mm PTFE substrate (Sterlitech Corporation, WA) by pulling 80 L of air per minute for 6 h on September 05, 2017, at the Environmental Molecular Sciences Laboratory of the Pacific Northwest National Laboratory (Richland, WA) downwind of wildfires that burned in British Columbia, Canada, and Washington, USA. Trajectories extending 48 h into the past from the time that sample collection was concluded on September 05 were generated using Hybrid Single-Particle Lagrangian Integrated Trajectory (HYSPLIT) at 350, 1000, and 2000 m above ground level (Figure S1), which showed the aerosol sample to be representative of plumes that had intercepted or traveled in close vicinity of wildfires in the 2 days preceding collection. A quarter of the filter was immersed in analytical-grade acetonitrile (ACN) and shaken at 60 rpm for 90 min at ambient temperature and pressure. The filter was then discarded, and the liquid ACN-aerosol mixture was filtered with a 0.2-μm PTFE syringe filter to remove insoluble material. The filtrate thus obtained was maintained at 4 °C during storage and shipment until analysis. Samples were diluted 10-fold in 50:50 H_2O/ACN immediately before analysis.

Electrospray Ionization and Ultrahigh-Resolution Mass Spectrometry. *15-T FT-ICR MS.* Spectra were acquired on a Bruker SolariX XR FT-ICR MS equipped with a ParaCell and actively shielded 15-T superconducting magnet. Samples were infused at 5 μL/min into an Apollo II ESI source operating in negative mode with a capillary voltage of 4 kV, dry gas flow of 4 L/min, temperature of 180 °C, and nebulizer gas pressure of 1 bar. The Q1 mass was set to m/z 100. Ions were accumulated for 150 ms before transfer to the analyzer cell with a time of flight of 0.75 ms. All spectra were acquired between m/z 153.6 and 1200.0 into an 8 MWord time domain with a transient length of 2.8 s. Three hundred transients were co-added before zero filling and Fourier transformation. The measured RP was ∼1 000 000 at m/z 400. Spectra were peak-picked in Data Analysis 5.0 (Bruker Daltonics, Billerica, MA) with an S/N threshold of 4.0 and absolute abundance threshold of 1 000 000, and peak lists were exported as .csv format for further data processing and formula assignment.

21-T FT-ICR MS. Spectra were acquired on a custom-built 21-T FT-ICR MS at PNNL, Richland, WA. Briefly, a Velos Pro linear ion trap front end was used for ionization and system control of a custom-built ICR flight tube and analyzer cell.[25] Samples were infused at 4 μL/min into a heated ESI (HESI) source (45 °C) with a spray voltage of 3.4 kV in negative mode. Eight arbitrary units of sheath gas were used to aid in nebulization. Inlet capillary temperature was set to 300 °C. An AGC target of 5×10^5 was set with a typical ion injection time of 5 ms. Spectra were recorded between m/z 150 and 800 a transient length of 1.5 s and target RP of ∼600 000 at m/z 400 (measured RP = ∼620 000) in magnitude-mode FT (mFT). One thousand broadband scans were recorded with single microscan events. Data were acquired with the FTMS Booster (Spectroswiss) data acquisition system allowing for post-acquisition co-addition of raw transients and absorption-mode Fourier transform (aFT) processing, yielding improved RP (measured RP = ∼1 200 000 at m/z 400) and sensitivity. Spectra with a width of 30 m/z units (3 s transient length) were also obtained by recording 100 narrow scanning ion monitoring (SIM) scans (1 microscan event per scan) centered at m/z 393 (m/z 378.06−405.26). The measured RP for SIM scanning was ∼2 200 000 at m/z 400. Peak-by-Peak (Spectroswiss) was used to co-add, Fourier transform, and phase-correct all scans. The mass spectrum was then peak-picked based on logarithmic noise thresholding with a noise value of

https://doi.org/10.1021/acs.analchem.2c00916
Anal. Chem. 2022, 94, 14537−14545

6.0, and the mass list was exported in .csv format for further data processing and formula assignment.

Data Processing and Molecular Formula Assignment. Mass lists acquired and exported from either instrument were subjected to further noise estimation using the KMDNoise() function in MFAssignR[28] to remove any residual noise. Monoisotopic and polyisotopic peaks were acquired from IsoFiltR(), followed by the selection of CH_2-homologous series as recalibration points from within the data set using Recal() to correct any systematic error in measured ion masses (Table S1). Molecular formulae were assigned to recalibrated *m/z* values using MFAssign() with the following constraints: $C_cH_hO_oN_{0-3}S_{0-1}P_{0-1}{}^{13}C_{0-2}{}^{34}S_{0-1}$ (numbers of C, H, and O were unrestricted); $-13 \leq$ DBE-O ≤ 20; $0 \leq$ O/C ≤ 2.0; $0.3 \leq$ H/C ≤ 2.5; and maximum permissible error of ±0.5 ppm. A *de novo* cutoff of *m/z* 350 was applied, whereby the unique elemental composition is calculated till *m/z* ≤ 350, and higher *m/z* values are assigned by their extension as homologous series of CH_2, O, H_2, H_2O, and CH_2O.[28] Unless otherwise indicated, assignments containing $^{13}C_{1-2}$ and/or ^{34}S atoms are not included in our discussion, considering that they are isotopic counterparts of monoisotopic formulae. Peak abundances were normalised to the abundance of the tallest peak. Structural information was inferred by calculating double bond equivalence (DBE) and modified aromaticity index (AI_{mod}),[18,19] where DBE = C + 1-H/2 + N/2 + P/2 and AI_{mod} = (1 + C-1/2O−S-1/2(N + H + P))/(C-1/2O−N−S−P). In both equations, C, H, O, N, S, and P are the numbers of atoms of these elements. The data processing pipeline (Code S1) is made available in the Supporting Information.

Chemical Imaging and Microanalysis of Single Particles. The atmospheric aerosol sample was collected onto 300-mesh transmission electron microscopy (TEM) grids coated with carbon type-B films (Ted Pella, Inc., CA) using a 10-stage micro-orifice uniform deposition impactor (MOUDI; Model 110-R, MSP, Inc.). For chemical imaging and microanalysis, we focused on samples that were collected on stages 7 (0.32−0.56 μm) and 8 (0.18−0.32 μm). Computer-controlled scanning electron microscopy with energy-dispersive X-ray (CCSEM/EDX) was used for the analysis of individual particles' elemental composition. X-ray spectra were acquired for 10 s of live time at an accelerating voltage of 20 kV and beam current of ∼430 pA. The elemental concentration of P was measured as an atomic percentage along with C, N, O, Na, Mg, Al, Si, S, Cl, K, Ca, Mn, Fe, and Zn. More than 3500 individual particles were analyzed. In addition, an aberration-corrected scanning transmission electron microscope (FEI Titan) coupled with an energy-dispersive X-ray spectrometer operated at 3000 kV was used to image single particles. Electron detection was performed using the high-angle annular dark-field detector. An EDX detector (Oxford Instruments) was used for the chemical imaging of particles.

RESULTS AND DISCUSSION

Overview of Molecular Composition. BBOA is polydisperse and multifunctional with C, H, O, N, S, and P elements present with various combinations of hydroxyls, carboxyl, carbonyl, and ester functionalities and often include nitrate, sulfate, or phosphate end members.[16,29−31] The chemical richness of ambient aerosols results from the combination of primary organic components emitted directly from the sources and secondary multiphase oxidative components that are formed as the air mass ages. In our wildfire-influenced BBOA sample, 6053 monoisotopic and 1383 polyisotopic ($^{13}C_{1-2}$ and/or ^{34}S) formulae belonging to CHO, CHNO, and CHOS molecular groups were assigned to peaks detected with the 15-T FT-ICR MS. The 21-T FT-ICR MS yielded 10 533 monoisotopic and 3420 polyisotopic formulae that belonged to CHO, CHNO, CHOS, CHOP, and CHNOP molecular groups and constituted 91.5% of the detected peaks. Here, CHOP and CHNOP species were exclusively observed in the 21-T FT-ICR MS analysis and comprised 4.6% (n = 488) and 2.0% (n = 244) of all formulae assigned, respectively. The numbers of peaks detected using the 15-T and the 21-T FT-ICR instruments and a summary of the nature of formulae assigned to them, including assignment errors (Figure S2), are presented in Table 1. A full list of formulae from both instruments is given in Data set S1. Centroid mass spectra of the unambiguously assigned monoisotopic formulae are drawn in Figure 1. A total of 11 474 peaks denoting distinct molecular formulae are shown in the reconstructed mass spectra, where the largest fraction of assigned formulae in both FT-ICR analyses belonged to CHNO species (∼50%), with CHO species being a close second. Regardless of the varying peak abundance distributions, both mass spectra in Figure 1 represent a similar molecular class distribution in the assigned formulae. Species containing O_2−O_{18}, NO_3−NO_{18}, N_2O_3−N_2O_{16}, and O_5S−$O_{12}S$ were detected by both instruments (Figure S3). A greater number of formulae were assigned to each class by the 21-T FT-ICR MS, along with the detection of additional classes ranging from N_3O_4−N_3O_{14}. A detailed description of these molecular classes (i.e., CHO, CHNO, and CHOS) is presented in Text S1, while the discussion that follows pertains exclusively to CHOP and CHNOP constituents.

In a recent analysis of pyrogenic organic matter in soil with 21-T FT-ICR MS using (+)ESI, Roth et al. demonstrated enhanced speciation of nitrogen-containing organic compounds.[32] Here, (−)ESI analysis using the 21-T FT-ICR MS led to novel CHOP or CHNOP formula assignments. Peaks corresponding to these species had very low abundances relative to those of other molecular groups (1−5% of the base peak)—which is not necessarily indicative of the minute quantities of organophosphorus compounds in the complex mixture but could be due to the inefficient ionization of $PO_4{}^{3-}$ groups by ESI as well.[20] To be sure of our findings, the P-containing formulae were tested against multiple formula assignment candidates before being finalized as the most suitable assignment. First, CHOP and CHNOP formulae had very low mean absolute formula error of 0.08 ± 0.04 ppm. Nearly all P-containing peaks reported here could also be assigned a $CHO^{32}S$ formula. However, such CHOS formulae were ruled out due to their unusual error patterns depicted in Figure S4 and their highly condensed nature (H/C and O/C <0.5), which is not a characteristic of organosulfur compounds in BBOA. Second, other possibilities, such as the inclusion of $^{35}Cl/^{37}Cl$ adducts, polyisotopic peaks (^{18}O, ^{15}N, etc.), or odd-electron ions in the formula assignment parameters, did not yield alternatives at an error tolerance of ≤0.5 ppm.

^{13}C Isotopic Fine Structure of Peaks Assigned CHOP or CHNOP Formulae. Isotopic fine structure involving ^{13}C was assessed to not only have additional confidence in CHOP and CHNOP assignments (note P is not a polyisotopic element) but also to highlight the analytical strength of the 21-T FT-ICR MS for complex mixtures. Dedicated SIM

https://doi.org/10.1021/acs.analchem.2c00916
Anal. Chem. 2022, 94, 14537−14545

Table 1. Summary of Bulk Chemical Metrics Based on Molecular Formulae Assigned to the Organic Aerosol Sample[a]

	total number of peaks	total number of peaks above S/N threshold	unassigned peaks	assigned monoisotopic formulae[b]	oxygen-to-carbon ratio, O/C_{avg}	hydrogen-to-carbon ratio, H/C_{avg}	double bond equivalence, DBE_{avg}	mass/charge, m/z_{avg}	absolute error (ppm), AE_{avg}	modified aromaticity index, $AI_{mod,avg}$
15-T FT-ICR MS										
all MF	23 701	9939	2447	6053	0.56 ± 0.2	1.19 ± 0.3	9.38 ± 4.4	430.85 ± 117.8	0.066 ± 0.05	0.29 ± 0.5
CHO				2618	0.48 ± 0.2	1.12 ± 0.3	10.30 ± 4.3	433.98 ± 126.6	0.063 ± 0.05	0.33 ± 0.2
CHNO				3080	0.60 ± 0.2	1.22 ± 0.3	9.20 ± 4.1	441.47 ± 107.1	0.066 ± 0.05	0.27 ± 0.6
CHOS				355	0.75 ± 0.3	1.49 ± 0.3	4.00 ± 2.6	315.56 ± 68.4	0.077 ± 0.05	0.12 ± 0.6
21-T FT-ICR MS										
all MF	34 557	15312	1294	10 533	0.46 ± 0.2	1.23 ± 0.3	10.38 ± 4.8	474.06 ± 124.2	0.032 ± 0.03	0.28 ± 0.3
CHO				4629	0.39 ± 0.2	1.22 ± 0.3	10.80 ± 5.0	483.06 ± 136.2	0.027 ± 0.02	0.30 ± 0.2
CHNO				5022	0.45 ± 0.2	1.17 ± 0.2	11.18 ± 4.0	474.43 ± 116.6	0.031 ± 0.03	0.29 ± 0.2
CHOS				190	0.70 ± 0.3	1.64 ± 0.2	3.22 ± 1.8	324.00 ± 64.7	0.026 ± 0.02	0.06 ± 0.5
CHOP				488	0.83 ± 0.2	1.75 ± 0.3	3.66 ± 2.2	455.93 ± 65.6	0.078 ± 0.04	0.00
CHNOP				204	1.02 ± 0.2	1.78 ± 0.2	3.74 ± 1.9	444.05 ± 57.2	0.077 ± 0.04	0.13 ± 1.3

[a]Considering that the peak abundance distributions and signal-to-noise ratio recorded by the two instruments differed considerably, number averages and standard deviations are reported. For reference, corresponding averages weighted to peak abundance are presented in Table S2. [b]Number of formulae assigned to monoisotopic peaks with ^{12}C, ^{1}H, ^{16}O, ^{14}N, ^{32}S, and ^{31}P only.

experiments were performed to observe polyisotopic peaks for low-abundance monoisotopic peaks, which were otherwise difficult to observe in broadband acquisitions. Scans acquired for m/z segments of a few units' lengths reduce the number of ions that are collected and passed on by the quadrupole mass filter to the ICR cell. Such SIM with longer transients increases sensitivity, RP, and mass accuracy, thereby improving the chances of polyisotopes and other minor constituents to be observed. This approach has previously been applied for the measurement of isotopic abundance and confirmation of formula assignments.[33−35] Here, a narrow SIM spectrum obtained in aFT mode (m/z 378.06−405.26; measured RP = 2 200 000 at m/z 400; number of scans = 100) yielded 54 monoisotopic CHOP formulae, of which 20.4% (n = 11) had their corresponding isotopic peak detected with up to two ^{13}C atoms. In comparison, in the broadband aFT spectrum (observed RP at m/z 400 = 1 200 000; number of scans = 1000), only two of the 55 monoisotopic CHOP species (3.6%) in the same m/z range had a corresponding $^{13}C_{1-2}$ isotopic peak detected. The boost in S/N in the SIM scan for commonly detected species was ∼1.3×. The tallest CHOP isotopic peak in the SIM spectrum, $^{13}C^{12}C_{13}H_{21}O_{11}P$, was observed with a relative abundance of only 2.4% and an S/N of 1.46. Correspondingly, this peak was not observed in the broadband spectrum.

Figure 2 shows a SIM spectrum for three monoisotopic CHOP peaks at m/z 397 with corresponding M + 1 and M + 2 positions. Here, $C_{15}H_{27}O_{10}P$ was the tallest CHOP peak (9.9% relative abundance) and, thus, presented a higher likelihood of an observable isotopic peak. Two isotopic peaks at M + 2, $^{13}C^{12}C_{13}H_{23}O_{11}P$, and $^{13}C^{12}C_{14}H_{27}O_{10}P$ were assigned with ∼0.06 ppm absolute formula error at relative abundances of 1.8 and 2.2%, respectively, and at measured RPs of 1 700 000 and 2 200 000 (Figure 2). The former was present at a 1.1% relative abundance and a measured RP of 1 100 000, while the latter was undetected in the broadband scan. Thirty-three CHNOP formulae were assigned in the SIM spectrum but with no isotopic peaks. This could be explained by the fact that the tallest CHNOP peak had a relative abundance of only 4.9% and 15 C atoms, which would place its ^{13}C isotopic peak below the S/N threshold.

Molecular Composition of Organophosphorus Compounds. The presence of P in atmospheric aerosol has been explored in numerous studies,[9,10,36,37] but its molecular characterization is essentially missing. Spectromicroscopy analyses indicated ∼8% of the total particulate matter in the BBOA sample to contain P (>0.5 atomic percentage), as shown in Figure S5. Molecular characterization with the 21-T FT-ICR MS produced 488 and 204 CHOP and CHNOP formulae, respectively. Despite the magnitude of molecular-level information obtained here from ultra-HRMS, exact (compound or structural) identification is a challenge due to the isomeric complexity of complex mixtures. Graphical tools, such as the Kendrick mass defect (KMD) plots or the Van Krevelen diagrams, cannot differentiate between isomers but are nonetheless valuable to make sense of mixtures with many unknowns, such as the complex BBOA analyzed here, via broad classifications and molecular-level repeating patterns.[31,38] In addition, trends and series in the KMD and VK diagrams are formed merely based on formulae assigned and do not imply similarity in structure.

Figure S6 shows the distribution of the number of C and O atoms, as well as the DBE, across the entire range of species

https://doi.org/10.1021/acs.analchem.2c00916
Anal. Chem. 2022, 94, 14537−14545

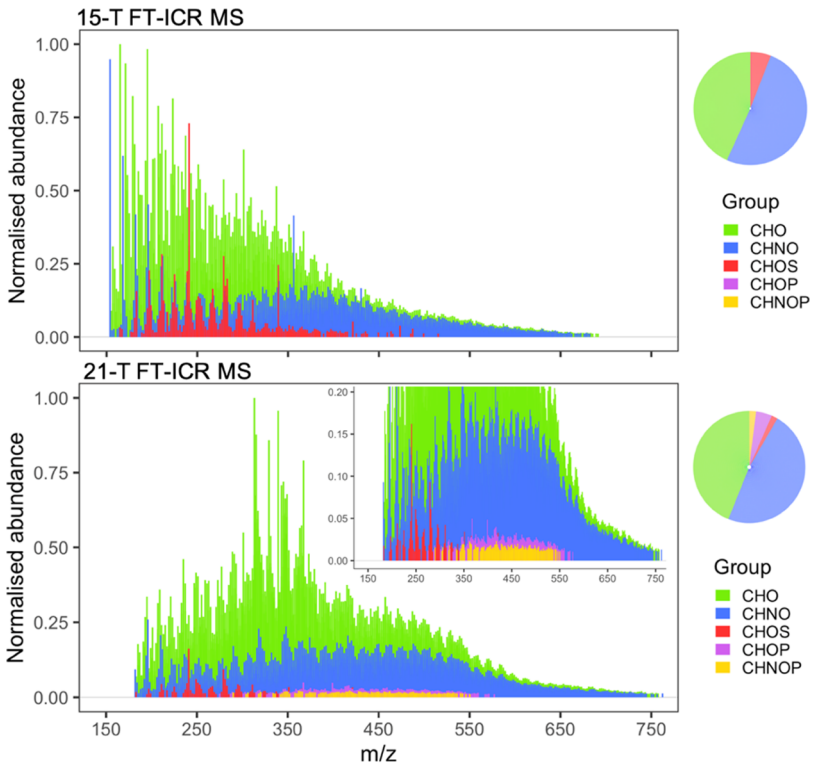

Figure 1. Reconstructed mass spectra of organic aerosols from (−)ESI analysis with 15-T and 21-T FT-ICR mass spectrometers. A vertical expansion of the latter spectrum is presented in the inset to aid the visualization of the low-abundance CHOP and CHNOP peaks. Peaks are colored by the molecular group of the formula assigned to them.

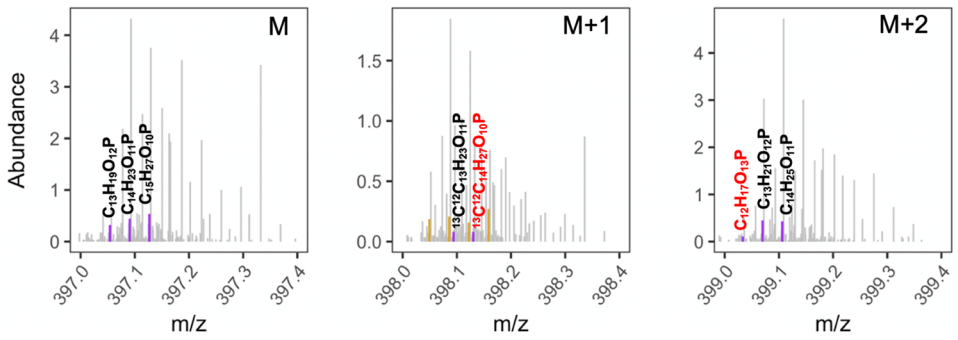

Figure 2. Reconstructed mass spectra from a selected ion monitoring scan showing peaks assigned CHOP formulae at m/z 397 (M). Corresponding polyisotopic peaks at positions M + 1 and M + 2 are drawn too. Peaks annotated in red font were not observed in the broadband scan.

detected. As compared to formulae that contained only C, H, O, N, and/or S, organophosphorus species had much smaller C skeletons of C_{7-24} (versus C_{7-41}). They were distributed across a continuum of O_oP_p and $N_nO_oP_p$ classes ($O_7P-O_{18}P$ and $NO_9P-NO_{17}P$), as shown in Figure 3C,D. Despite smaller C skeletons, CHOP or CHNOP formulae could be organized into 64 and 40 KMD homologous series with CH_2 as the base. Figure 3A,B depicts a portion of the CHOP and CHNOP formula assignments and pinpoints the KMD series lying therein with the corresponding DBE. Most KMD series of CHOP and CHNOP formulae had ≥7 and ≥4 members, respectively (Figure S7). According to Figure S7, longer KMD series were dominated by low DBE values of <5. In the case of CHOP, the longest KMD series had 14 members (represented as C5 in Figure 3A), with $C_{10}H_{17}O_{13}P$ as the core (smallest) molecule. With a DBE of 3, this series could comprise P-containing species with either three double bonds or a ring with two double bonds. The second-longest series had 13 members, each starting from $C_9H_{15}O_{12}P$ (DBE = 3) and $C_{11}H_{17}O_{12}P$ (DBE = 4) as the core molecules. The highest unsaturation of DBE = 9 was exhibited by only one 3-membered series starting with $C_{18}H_{21}O_{13}P$. A predominance of CHOP species with low degrees of unsaturation and low AI_{mod}[18,19] values (classified into aliphatic groups) suggested the presence of compounds resembling phospholipids or phosphate sugars. The longest KMD series in the CHNOP group was 9-membered and started from $C_9H_{16}NO_{13}P$ (DBE = 3). The second-longest series had 8 members, each starting from $C_8H_{16}NO_{13}P$ (DBE = 2) and $C_7H_{16}NO_{13}P$ (DBE = 1) as the core molecules. The highest unsaturation of DBE = 7 was exhibited by two 4-membered KMD series starting with $C_{16}H_{22}NO_{13}P$ and $C_{16}H_{22}NO_{14}P$.

Similar to the KMD plots, van Krevelen (VK) diagrams organize species in characteristic trend lines to represent

https://doi.org/10.1021/acs.analchem.2c00916
Anal. Chem. 2022, 94, 14537−14545

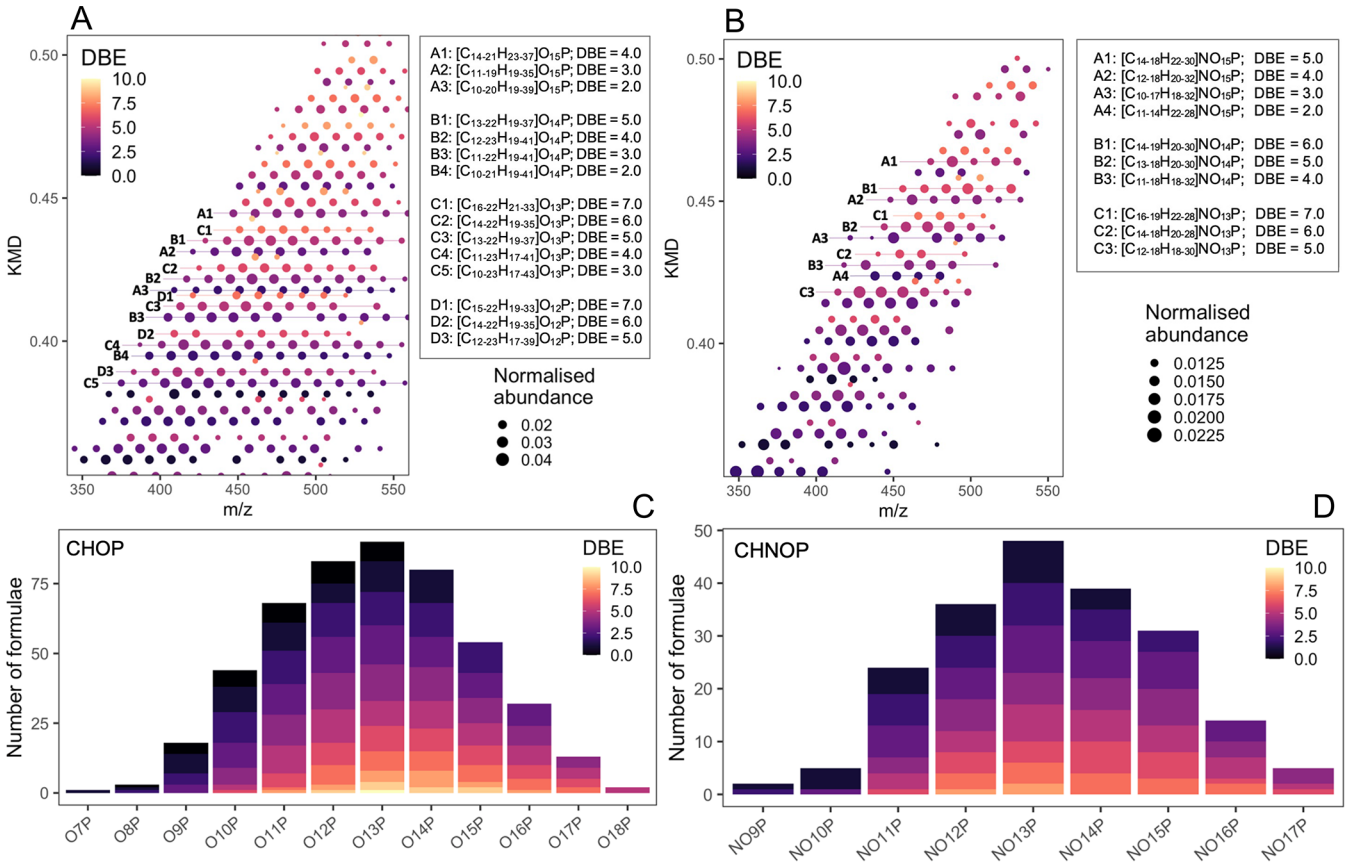

Figure 3. Molecular characteristics and classes of CHOP and CHNOP formulae detected in the organic aerosol sample. (A, B) Zoomed-in Kendrick mass defect plot with CH_2 as the base, where data points are colored by double bond equivalence. Elemental compositions of representative CH_2-homologous series are elaborated in the adjacent table. The number and length of all homologous series formed by the CHOP and CHNOP species are drawn in Figure S7. (C, D) Frequency of occurrence of formulae in P-containing heteroatomic classes, O_oP and NO_oP.

possible reaction pathways relating them to one another (Figure S8), such as hydration/condensation, de/hydrogenation, oxidation/reduction, and methylation/demethylation.[38−40] In the VK space, both P-containing molecular groups occupied regions of higher oxygenation and hydrogen saturation as compared to CHO and CHNO species (Figure S9). Tu et al.[41] suggest molecular species with O/C ≥ 0.6 to be highly oxidized and those with H/C > 1.2 to be highly saturated. Both CHOP and CHNOP formulae were reflective of oxygenated, aliphatic species as they had some of the highest numbers of O atoms as compared to the rest of the data set (O_{9-18} versus O_{1-19}) and the lowest DBE values (0−9 versus 1−24), as shown in Figure S7.

To gain deeper insight into the possible compound classes of P-containing species in this BBOA sample, formulae assigned were manually compared to known compounds curated at ChemSpider,[42] which yielded more than one match for 127 (26.1%) CHOP and 19 (8.8%) CHNOP formulae. In total, there were 402 and 70 matches for the two molecular groups, respectively, that included metabolites, such as PO_4^{3-} mono and diesters in phospholipids, phosphamides, phosphoproteins, inositol, sugar phosphates, etc. Structures that matched with CHNOP included phosphorylated amino acid residues and amino sugars. Monoesters and diesters could also be decomposition products of nucleic acids and lipids.[14] Furthermore, an estimate of the lability of organic matter in complex mixtures places bioavailable material at H/C ≥ 1.5,[43] according to which all P-containing molecular compounds detected and assigned a formula here were likely bioavailable species, such as phosphorylated amino sugars or carbohydrates.

Molecular formulae can help infer compound classes and functionalities based on the ratio of heteroatoms as well. For instance, a molecular O/N ratio of ≥3 in BBOA has been associated with NO_2 (nitro) or NO^{3-} (nitrate) functional groups.[16,44] Similarly, O/S ≥ 4 suggests the presence of SO_3^{2-} (sulfite), SO_4^{2-} (sulfate), or HSO^{3-} (sulfonic) functional groups.[44] These are reasonable inferences that have been supported by fragmentation studies reporting associated neutral losses, such as HNO_3,[45,46] HNO_2, and NH_3[46] in atmospheric OA. The low relative abundances of peaks assigned CHOP or CHNOP in this study prevented their isolation for fragmentation studies. Regardless, molecular O/P values of ≥7 and O/P_{avg} of 12.80 ± 2.0 in formulae suggested that CHOP species had at least seven O atoms available for each P, allowing for the possibility of $-OPO_3$ with other O-based functionalities. Similarly, the values of O/(P + N) were ≥4.5 with $[O/(P + N)]_{avg}$ of 6.64 ± 0.83, suggesting the possibility of CHNOP species to have both $-OPO_3$ with reduced N groups, such as NH_2, as well as NO (nitroso), NO_2, or NO^{3-} with other O-based functionalities. Currently, no studies on the molecular composition of organophosphorus compounds in the atmospheric aerosol are available to support these speculations or to provide tentative structural information. Therefore, future research must focus on elucidating the structures of these compounds by performing tandem MS analysis.

https://doi.org/10.1021/acs.analchem.2c00916
Anal. Chem. 2022, 94, 14537−14545

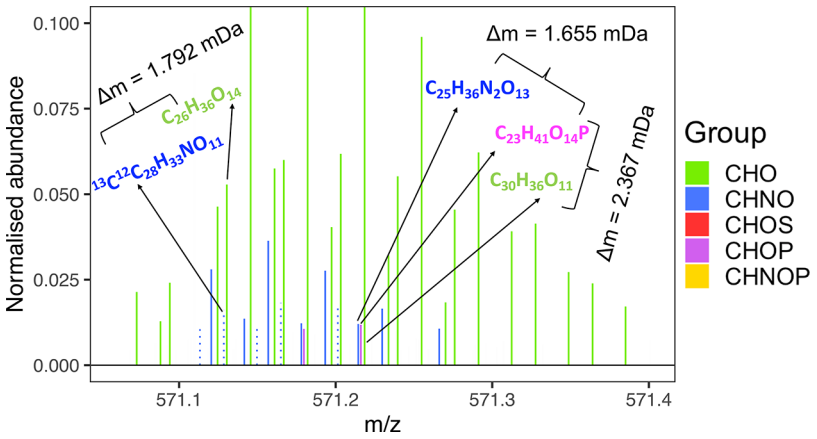

Figure 4. Reconstructed mass spectra at *m/z* 571 from (−)ESI/21-T FT-ICR MS analysis. The spectrum has been zoomed in to aid in the visualization of low-abundance peaks. Delta masses of a few adjacent peaks are depicted with the resolving powers theoretically required to resolve them from adjacent peaks.

Differences in Mass Spectral Parameters of the FT-ICR Instruments: Resolution and Sensitivity. A previous study on the direct comparison between 9.4 and 21-T FT-ICR MS[27] reported heteroatomic classes with ≥3 O atoms to be assigned exclusively by the latter due to its ability to resolve H_3O_3 from $C_2N^{13}C$, i.e., Δm = 1.792 mDa, in a variety of complex environmental mixtures, benefiting the analysis of O-rich samples. Unless a deliberate effort is expended to acquire identical mass spectra for complex mixtures from different instruments, user-defined ionization and instrumental tune settings create biases in detection, which introduces variability in molecular composition and ion abundances,[47] Here, the same BBOA was characterized by independently optimizing signal and resolution on the 15-T and 21-T[25] FT-ICR MS, and thus, more work is needed to concretely attribute the observations presented in this section to differential instrument design and function in the future. Nonetheless, the apparent enhancement in performance of the 21-T FT-ICR MS was attributable to its better sensitivity toward species that were present in relatively small quantities in the sample rather than the greater RP at which data was acquired from it (1 200 000 at *m/z* 400 with aFT processing versus 1 000 000 at *m/z* 400 for the 15-T FT-ICR MS). For instance, the resolution of $C_{23}H_{41}O_{14}P$ from isobaric species, $C_{30}H_{36}O_{11}$ and $C_{25}H_{36}N_2O_{13}$, at *m/z* 571 required RPs of 239 000 and 342 000, respectively (Figure 4). The resolution of $C_{26}H_{36}O_{14}$ from $^{13}C^{12}C_{28}H_{33}NO_{11}$ at the same nominal mass required an RP of 308 000. The resolution of $C_{14}H_{27}O_{15}P$ from $^{13}C^{12}C_{23}H_{19}NO_9$ required an RP of 810 000 at *m/z* 465 (spectrum not shown). All of these ion pairs were resolvable by the 15-T FT-ICR MS, but they remained undetected. Another such observation was made in the detection of species assigned an O_7 formula, which was the most common heteroatomic class with only C, H, and O constituents (Figure S3). Juxtaposed spectra at three nominal masses (*m/z* 305, 401, and 505) drawn in Figure S11 show that not only did the commonly detected peaks have a higher S/N ratio in the 21-T FT-ICR MS analysis, but also at the highest *m/z*, none of the O_7 peaks were detected by the 15-T FT-ICR MS.

Better detection by the 21-T FT-ICR MS may likely be due to a much higher number of transients co-added for it (1000 as compared to 300 from the 15-T FT-ICR MS) to optimize data acquisition, other than its better sensitivity and dynamic range due to higher field strength. However, the number of scans was not the only decisive factor, as the S/N of 14.45% of the overlapping peaks (that were assigned a formula) between the two instruments was greater in the 15-T FT-ICR analysis than in the 21-T FT-ICR analysis. In addition, a small number of species (n = 941) were observed exclusively in the 15-T FT-ICR MS analysis and majorly comprised oxygenated (O/C > 0.5) N and S-containing species of low DBE <12 (Figure S10). Notably, ∼2400 unassigned peaks (10.32% of the raw mass list) that accounted for 15% of the cumulative ion abundance were enriched in the 15-T FT-ICR mass spectrum (gray peaks in Figure S12). The ions forming these peaks were either not detected by the 21-T FT-ICR MS or had very low S/N.

These unassigned peaks in the 15-T FT-ICR MS could be organized in CH_2-homologous series using KMD but could not be assigned molecular formulae with the routine used here. We could also not satisfactorily prove the presence of nontraditional elements/adducts (F, Cl, Na, etc.), odd-electron ions, multiple charges, etc. Considering that these species were observed only in BBOA samples, such as the one reported here and others to be reported elsewhere in the future, but not in other natural complex mixtures, including Suwannee River fulvic acid and Maple leaf organic matter extracts analyzed during the same experimentation period, we speculate that these unassigned species were likely unique to our BBOA and were not contaminants. As most instrumental settings and even data acquisition protocols (such as the use of aFT processing) caused an overall better sensitivity of the 21-T FT-ICR MS, differences observed in the molecular composition could have been contributed by numerous other instrumental design aspects that set the two mass spectrometers apart, such as their ESI sources, types of ICR cell, ion optics, etc., but are outside of the scope of this paper. Future research must attempt to concretely attribute such variability in molecular characterizations of BBOA and other complex mixtures to differential instrumental design and function.

CONCLUSIONS

We present the first molecular-level characterization of organophosphorus compounds with C, H, O, and P constituents, with or without N, in atmospheric BBOA originating from wildfires in the Pacific Northwest by ultrahigh-resolution mass spectrometry. These compounds were detected among a rich matrix of 9841 non-P formulae

https://doi.org/10.1021/acs.analchem.2c00916
Anal. Chem. 2022, 94, 14537−14545

belonging to three molecular groups: CHO, CHNO, and CHOS. Although CHOP and CHNOP groups formed only 6.57% of all assigned formulae, they are extremely environmentally relevant due to their tendency for incorporation into the nutrient load of aquatic ecosystems, leading to substantial changes in the biogeochemical balance. It is, therefore, essential that they be included in the careful exploration of wildfire-influenced organic aerosols to better understand their downwind fate and implications. Our results demonstrate the utility of ultra-HRMS with the 21-T FT-ICR MS for the detection and identification of organophosphorus compounds in BBOA and potentially other minor constituents as well without their pretreatment or selective concentration from the non-P organic matrix. With the increased frequency of wildfires and other large-scale biomass burning episodes expected globally in the future, it is crucial to explore all possible avenues that can advance our understanding of atmospheric aerosols and their interaction with ecosystems.

■ ASSOCIATED CONTENT

Supporting Information

The Supporting Information is available free of charge at https://pubs.acs.org/doi/10.1021/acs.analchem.2c00916.

Code S1, R code for formula assignment (PDF)

Data set S1, all formulae assigned by 15-T and 21-T FT-ICR MS analysis (XLSX)

Backward trajectory of wind plumes; error distribution; class distributions; phosphorus content by atomic percentage; distribution of formulae; number and length of CH_2-homologous series; arrangement of CHOP and CHNOP species; molecular species identified exclusively or commonly by 15-T and 21-T FT-ICR mass spectrometers; reconstructed mass spectra at nominal masses (Figures S1−S12); recalibrant series used to correct systematic bias in the exact masses of ion; and summary of bulk chemical metrics based on molecular formulae assigned to the organic aerosol sample (Tables S1 and S2) (PDF)

■ AUTHOR INFORMATION

Corresponding Authors

Amna Ijaz − *Department of Chemistry, Michigan Technological University, Houghton, Michigan 49931, United States;* orcid.org/0000-0001-8727-7739; Email: aijaz@mtu.edu

Lynn R. Mazzoleni − *Department of Chemistry, Michigan Technological University, Houghton, Michigan 49931, United States*; Email: lrmazzol@mtu.edu

Authors

William Kew − *Environmental Molecular Sciences Laboratory, Pacific Northwest National Laboratory, Richland, Washington 99354, United States;* orcid.org/0000-0002-4281-4630

Swarup China − *Environmental Molecular Sciences Laboratory, Pacific Northwest National Laboratory, Richland, Washington 99354, United States;* orcid.org/0000-0001-7670-335X

Simeon K. Schum − *Department of Chemistry, Michigan Technological University, Houghton, Michigan 49931, United States*

Complete contact information is available at: https://pubs.acs.org/10.1021/acs.analchem.2c00916

Author Contributions

The manuscript was written through the contributions of all authors. The sample was collected and prepared by S.C. and S.K.S. Mass spectrometric data were collected and preprocessed by W.K. Mass spectrometric data were post-processed and analyzed by A.I. The project was awarded to and supervised by L.R.M.

Notes

The authors declare no competing financial interest.

■ ACKNOWLEDGMENTS

The authors would like to thank the two anonymous reviewers for their careful reading of our manuscript and their many constructive comments and suggestions. This research was performed on a project award (https://doi.org/10.46936/lser.proj.2019.50795/60000103) from the Environmental Molecular Sciences Laboratory, a DOE Office of Science User Facility sponsored by the Biological and Environmental Research Program under Contract No. DE-AC05-76RL01830. The authors also acknowledge support from the US Department of Energy (DE-SC0021168). A.I. was supported by a Fulbright Foreign Student Exchange Program by the US Department of State. A.I. also extends thanks to Subuktageen Qitta for his intellectual input that greatly helped improve the process of compiling this report.

■ REFERENCES

(1) Rockström, J.; Steffen, W.; Noone, K.; Persson, Å.; Chapin, F. S.; Lambin, E. F.; Lenton, T. M.; Scheffer, M.; Folke, C.; Schellnhuber, H. J.; et al. *Nature* **2009**, *461*, 472−475.

(2) Zhou, S.; Collier, S.; Jaffe, D. A.; Briggs, N. L.; Hee, J.; Sedlacek, A. J., III; Kleinman, L.; Onasch, T. B.; Zhang, Q. *Atmos. Chem. Phys.* **2017**, *17*, 2477−2493.

(3) Garofalo, L. A.; Pothier, M. A.; Levin, E. J.; Campos, T.; Kreidenweis, S. M.; Farmer, D. K. *ACS Earth Space Chem.* **2019**, *3*, 1237−1247.

(4) Gunsch, M. J.; May, N. W.; Wen, M.; Bottenus, C. L.; Gardner, D. J.; VanReken, T. M.; Bertman, S. B.; Hopke, P. K.; Ault, A. P.; Pratt, K. A. *Atmos. Chem. Phys.* **2018**, *18*, 3701−3705.

(5) Palm, B. B.; Peng, Q.; Fredrickson, C. D.; Lee, B. H.; Garofalo, L. A.; Pothier, M. A.; Kreidenweis, S. M.; Farmer, D. K.; Pokhrel, R. P.; Shen, Y.; et al. *Proc. Natl. Acad. Sci. U.S.A.* **2020**, *117*, 29469−29477.

(6) Tipping, E.; Benham, S.; Boyle, J.; Crow, P.; Davies, J.; Fischer, U.; Guyatt, H.; Helliwell, R.; Jackson-Blake, L.; Lawlor, A. J.; et al. *Environ. Sci.: Process. Impacts* **2014**, *16*, 1608−1617.

(7) Anderson, L.; Faul, K.; Paytan, A. *Mar. Chem.* **2010**, *120*, 44−56.

(8) Prospero, J.; Barrett, K.; Church, T.; Dentener, F.; Duce, R.; Galloway, J.; Levy, H.; Moody, J.; Quinn, P. Atmospheric Deposition of Nutrients to the North Atlantic Basin. In *Nitrogen Cycling in the North Atlantic Ocean and its Watersheds*, Springer, 1996; pp 27−73.

(9) Sundarambal, P.; Balasubramanian, R.; Tkalich, P.; He, J. *Atmos. Chem. Phys.* **2010**, *10*, 11323−11336.

(10) Wang, R.; Balkanski, Y.; Boucher, O.; Ciais, P.; Peñuelas, J.; Tao, S. *Nat. Geosci.* **2015**, *8*, 48−54.

(11) Newman, E. I. *J. Ecol.* **1995**, *83*, 713−726.

(12) Graham, W. F.; Duce, R. A. *Atmos. Environ.* **1982**, *16*, 1089−1097.

(13) Tsukuda, S.; Sugiyama, M.; Harita, Y.; Nishimura, K. *Biogeochemistry* **2006**, *77*, 117−138.

(14) Myriokefalitakis, S.; Nenes, A.; Baker, A. R.; Mihalopoulos, N.; Kanakidou, M. *Biogeosciences* **2016**, *13*, 6519−6543.

(15) Boucher, O.; Randall, D.; Artaxo, P.; Bretherton, C.; Feingold, G.; Forster, P.; Kerminen, V.-M.; Kondo, Y.; Liao, H.; Lohmann, U.;

Rasch, P.; Satheesh, S. K.; Sherwood, S.; Stevens, B.; Zhang, X. Y. Clouds and Aerosols. In *Climate Change 2013: The Physical Science Basis: Working Group I Contribution to the Fifth Assessment Report of the Intergovernmental Panel on Climate Change* Stocker, T.; Qin, D.; Plattner, G. K.; Tignor, M.; Allen, S. K.; Boschung, J.; Nauels, A.; Xia, Y.; Bex, V.; Midgley, P. M., Eds.; Cambridge University Press: Cambridge, 2014.
(16) Willoughby, A. S.; Wozniak, A.; Hatcher, P. G. *Atmos. Chem. Phys.* **2014**, *14*, 10299−10314.
(17) Wozniak, A.; Bauer, J.; Sleighter, R.; Dickhut, R.; Hatcher, P. *Atmos. Chem. Phys.* **2008**, *8*, 5099−5111.
(18) Koch, B. P.; Dittmar, T. *Rapid Commun. Mass Spectrom.* **2006**, *20*, 926−932.
(19) Koch, B. P.; Dittmar, T. *Rapid Commun. Mass Spectrom.* **2016**, *30*, 250.
(20) Llewelyn, J. M.; Landing, W. M.; Marshall, A. G.; Cooper, W. T. *Anal. Chem.* **2002**, *74*, 600−606.
(21) Cooper, W. T.; Llewelyn, J. M.; Bennett, G. L.; Salters, V. J. *Talanta* **2005**, *66*, 348−358.
(22) Kurek, M.; Harir, M.; Shukle, J.; Schroth, A.; Schmitt-Kopplin, P.; Druschel, G. *Anal. Chim. Acta* **2020**, *1130*, 29−38.
(23) Dibley, M.; Jaffe, A.; O'Brien, R. E. *ACS Earth Space Chem.* **2022**, *6*, 775−787.
(24) Hendrickson, C. L.; Quinn, J. P.; Kaiser, N. K.; Smith, D. F.; Blakney, G. T.; Chen, T.; Marshall, A. G.; Weisbrod, C. R.; Beu, S. C. *J. Am. Soc. Mass Spectrom.* **2015**, *26*, 1626−1632.
(25) Shaw, J. B.; Lin, T.-Y.; Leach, F. E., III; Tolmachev, A. V.; Tolić, N.; Robinson, E. W.; Koppenaal, D. W.; Paša-Tolić, L. *J. Am. Soc. Mass Spectrom.* **2016**, *27*, 1929−1936.
(26) Marshall, A. G.; Guan, S. *Rapid Commun. Mass Spectrom.* **1996**, *10*, 1819−1823.
(27) Smith, D. F.; Podgorski, D. C.; Rodgers, R. P.; Blakney, G. T.; Hendrickson, C. L. *Anal. Chem.* **2018**, *90*, 2041−2047.
(28) Schum, S. K.; Brown, L. E.; Mazzoleni, L. R. *Environ. Res.* **2020**, *191*, No. 110114.
(29) Dzepina, K.; Mazzoleni, C.; Fialho, P.; China, S.; Zhang, B.; Owen, R. C.; Helmig, D.; Hueber, J.; Kumar, S.; Perlinger, J. A.; et al. *Atmos. Chem. Phys.* **2015**, *15*, 5047−5068.
(30) Brege, M.; China, S.; Zelenyuk-Imre, A.; Mazzoleni, L. *ACS Earth Space Chem.* **2021**, *5*, 2729−2739.
(31) Laskin, A.; Smith, J. S.; Laskin, J. *Environ. Sci. Technol.* **2009**, *43*, 3764−3771.
(32) Roth, H. K.; Borch, T.; Young, R. B.; Bahureksa, W.; Blakney, G. T.; Nelson, A. R.; Wilkins, M. J.; McKenna, A. M. *Anal. Chem.* **2022**, *94*, 2973−2980.
(33) Kang, W.-Y.; Thompson, P. T.; El-Amouri, S. S.; Fan, T. W.; Lane, A. N.; Higashi, R. M. *Anal. Chim. Acta* **2019**, *1080*, 104−115.
(34) Kew, W.; Goodall, I.; Clarke, D.; Uhrín, D. *J. Am. Soc. Mass Spectrom.* **2017**, *28*, 200−213.
(35) Weber, R. J. M.; Southam, A. D.; Sommer, U.; Viant, M. R. *Anal. Chem.* **2011**, *83*, 3737−3743.
(36) Yu, L.; Ma, X.; Gao, H.; Zong, H.; Yao, X.; Lin, Z.; Zhang, Z.; Zhang, C.; Yao, X.; Zhang, Z. *Atmos. Environ.* **2020**, *234*, No. 117475.
(37) Furutani, H.; Meguro, A.; Iguchi, H.; Uematsu, M. *Geophys. Res. Lett.* **2010**, *37*, No. L03805.
(38) Kim, S.; Kramer, R. W.; Hatcher, P. G. *Anal. Chem.* **2003**, *75*, 5336−5344.
(39) D'Andrilli, J.; Foreman, C.; Marshall, A. G.; McKnight, D. *Org. Geochem.* **2013**, *65*, 19−28.
(40) Stenson, A. C.; Marshall, A. G.; Cooper, W. T. *Anal. Chem.* **2003**, *75*, 1275−1284.
(41) Tu, P.; Hall, W. A., IV; Johnston, M. V. *Anal. Chem.* **2016**, *88*, 4495−4501.
(42) Pence, H. E.; Williams, A. *J. Chem. Educ.* **2010**, *87*, 1123−1124.
(43) D'Andrilli, J.; Cooper, W. T.; Foreman, C. M.; Marshall, A. G. *Rapid Commun. Mass Spectrom.* **2015**, *29*, 2385−2401.
(44) Brege, M.; Paglione, M.; Gilardoni, S.; Decesari, S.; Facchini, M. C.; Mazzoleni, L. R. *Atmos. Chem. Phys.* **2018**, *18*, 13197−13214.
(45) LeClair, J. P.; Collett, J. L.; Mazzoleni, L. R. *Environ. Sci. Technol.* **2012**, *46*, 4312−4322.
(46) Schum, S. K. Molecular Characterization of Free Tropospheric Organic Aerosol and the Development of Computational Tools for Molecular Formula Assignment. Dissertation; Michigan Technological University: Houghton, MI, 2019.
(47) Hawkes, J. A.; D'Andrilli, J.; Agar, J. N.; Barrow, M. P.; Berg, S. M.; Catalán, N.; Chen, H.; Chu, R. K.; Cole, R. B.; Dittmar, T.; et al. *Limnol. Oceanogr. Methods* **2020**, *18*, 235−258.

https://doi.org/10.1021/acs.analchem.2c00916
Anal. Chem. 2022, 94, 14537−14545